Journal of Applied Polymer Science

Hydrophobic and nanoporous chitosan–silica composite aerogels for oil absorption

Qian Ma,[1,2] Yanfei Liu,[1,2] Zhe Dong,[1,2] Jianglang Wang,[1,2] Xin Hou[1,2]

[1]Tianjin Key Laboratory of Composite and Functional Materials, Tianjin 300072, People's Republic of China

[2]School of Materials Science and Engineering, Tianjin University

Correspondence to: X. Hou (E-mail: houxin@tju.edu.cn)

ABSTRACT: Hydrophobic and nanoporous chitosan–silica composite aerogels with low density, high porosity, and superior oil absorbency were successfully prepared by a typical sol–gel method and a two-step hydrophobic treatment. The morphologies, porosity characteristics, mechanical properties, thermal stability, hydrophobicity, and oil absorbencies of the composite aerogels were systematically investigated. The nitrogen physisorption analysis showed that composite aerogels had large specific surface areas and uniform nanoporous structures. In addition, the composite aerogels could support 7000 times its own weight; this indicated the role of the supporting skeleton played by chitosan. The hydrophobicity and lipophilicity was demonstrated with a water contact angle of 137° and an oil contact angle of 0°. Importantly, the composite aerogel with 20 wt % chitosan had a relatively high oil absorbency of 30 g/g and could be reused up to 10 times. Therefore, the chitosan–silica composite aerogels in this study had a broad prospect to be used as efficient and recyclable oil absorbents. © 2014 Wiley Periodicals, Inc. J. Appl. Polym. Sci. **2015**, *132*, 41770.

KEYWORDS: composites; gels; porous materials

Received 17 August 2014; accepted 15 November 2014

DOI: 10.1002/app.41770

INTRODUCTION

Aerogels are a novel kind of porous materials, which are characterized by low density, high porosity, large surface area, low acoustic impedance, low thermal conductivity, and high adsorption.[1] Because of these properties, aerogels have been extensively applied in many fields, including sensors, catalysts, absorbents, artificial muscles, electrode materials, and insulation materials.[2–10] Typically, aerogels can be categorized into organic aerogels,[11,12] inorganic aerogels,[13,14] carbonization aerogels,[15,16] and organic–inorganic composite aerogels.[17,18] Among the various kinds of aerogels, silica aerogels have been investigated widely for a long time because of their outstanding properties and facile preparation process.[19–21]

In recent years, some researches have revealed that silica aerogels have great prospects for use as oil absorbents. For example, Gurav *et al.*[22] prepared a silica aerogel with methyltrimethoxysilane as hydrophobic precursor, and it could absorb toluene at 12 times its own weight after supercritical point drying. In another instance, Parale *et al.*[23] used trimethylchlorosilane as a precursor and ambient pressure drying as the drying method to synthesize a silica aerogel with an oil absorbency of 14 g/g. Nevertheless, the development of silica aerogels for efficient oil absorbent material has still been at the initial stage; it has been mainly hindered by the low swelling capacity and inherent fragility of such materials. A novel kind of aerogels with improved swelling capacity, porosity, and mechanical properties for iterative uses is desirable.

Although the mechanical properties of silica aerogels can be enhanced with the addition of fillers (fiber, ceramic, metal, etc.), such improvements are usually accompanied by the huge sacrifice of other performances; this is contrary to the initial expectation. Consequently, to solve this problem, an effective supporting skeleton is necessary.

Among numerous materials, chitosan is a kind of unique polysaccharide composed of glucosamine units and *N*-acetyl glucosamine units,[24] with many favorable characteristics, including biocompatibility, biodegradability, nontoxicity, and chemical activity.[25] Because of these outstanding properties, chitosan can be selected as a useful and effective polymer matrix in composite materials. Moreover, its hydroxyl and amino groups are beneficial for the formation of hydrogen-bond interactions and homogeneous phases in composite structures; these provide chitosan with great advantages as a skeleton material. In addition, because of its chemical activity, chitosan-based aerogels offer new space for applications in the fields of oil absorption and heavy-metal-ion absorption.

In this study, a detailed and comprehensive study of the preparation and properties of hydrophobic chitosan–silica aerogels

was made for the first time. Using a certain amount of chitosan as a supporting skeleton, we successfully prepared chitosan–silica composite aerogels. Instead of the traditional complex and costly methods, a simple and feasible two-step hydrophobic treatment method was adopted to modify the composite aerogels to be hydrophobic but also oleophilic. In addition, the morphologies, porosity characteristics, mechanical properties, and oil absorbencies of the composite aerogels were systematically measured and studied.

EXPERIMENTAL

Materials

Tetraethoxysilane (TEOS; 99%) as a precursor and hexamethyl disilazane (HMDS; 99%) as a hydrophobic modifier were purchased from Tianjin Heowns Biochem Technologies LLC (Tianjin, China). Chitosan with a low viscosity (<200 mPa s) and high deacetylation degree (≥90%) was purchased from Aladdin Reagent Co., Ltd. (Shanghai, China). Pure acetic acid, oxalic acid dihydrate, *n*-hexane, absolute ethanol, pentane, acetone, butyl acetate, dichloromethane, and xylene were analytical reagents, and all of them were obtained from Tianjin Jiangtian Chemical Reagent Co., Ltd. (Tianjin, China). Gasoline and arachis oil were bought from market. Ammonia ($NH_3{\cdot}H_2O$, 25–28%) was provided by Tianjin Kemiou Chemical Reagent Co., Ltd. (Tianjin, China). Glutaraldehyde (>50%) was purchased from Tianjin Bodi Chemical Industry Co., Ltd. (Tianjin, China). All of the previous materials were used without further processing.

Preparation of Pure Silica Aerogels and Chitosan Aerogels

Pure silica aerogels were prepared typically through the hydrolysis and polycondensation of TEOS. First, 5 mL of TEOS was diluted in 30 mL of 60 vol % ethanol and hydrolyzed for 1 h under a pH of 3–4 by the addition of an 0.5 mol/L oxalic acid solution drop by drop. Then, 0.1–0.2 mL of a 1% diluted ammonia ($NH_3{\cdot}H_2O$) was added to the sols under continuous stirring until the pH reached 6–7. Gels were formed within 2 h and aged at 25°C for 2–3 h. Then, they were washed with deionized water to remove the impurities. Finally, silica aerogels were obtained by vacuum freeze drying (vacuum freeze-drying apparatus, Scientz-12N, China). The pure silica aerogels without the addition of chitosan were named 0-CS.

The pure chitosan aerogels were prepared with glutaraldehyde as the crosslinker. An amount of 0.23 g of chitosan was dissolved in 0.5 vol % acetic acid solution, and 0.5 mL of glutaraldehyde was added to the chitosan solution under vigorous stirring. The sols were formed immediately and then were poured into a polystyrene-cultivating disk. After the gelation and aging process, the unreacted glutaraldehyde and acetic acid in the wet gels were exchanged with absolute ethanol three times. The gels were immersed in deionized water for 24 h, and they were lyophilized finally. The pure chitosan aerogels were named 100-CS.

Preparation of Chitosan–Silica Composite Aerogels

In the first step, a certain amount of chitosan was dissolved thoroughly in a 0.5% acetic acid solution. The chitosan solution and TEOS solution were mixed together, and homogeneous viscous sols were formed under vigorous stirring for 12 h. Then, the sols were poured into a polystyrene–cultivating disk and aged for several hours. The composite gels were immersed into deionized water and were washed three times to remove the impurities. Finally, the composite aerogels were obtained after freeze drying. The composite aerogels with 5 wt % chitosan were named 5-CS, and the other samples were named in the same way.

Hydrophobic Treatment

The surface modification of aerogels was performed in two steps with HMDS as the modifier. The aerogels were modified to be hydrophobic because HMDS reacted with hydroxyl groups on the surface of aerogels, and the hydrophilic groups were replaced by alkyl groups. First, the wet gels were solvent-exchanged by a 10 vol % HMDS–hexane solution, and then, they were washed with absolute ethanol and deionized water successively. Second, the dried aerogels were exposed to HMDS vapors at 50°C for several hours to ensure the complete modification of the surface. Finally, the hydrophobic aerogels were obtained.

Characterization

X-ray Diffraction (XRD). The XRD study was carried out for phase analysis with an X-ray diffractometer (D8 Advanced, Bruker, Germany) with Cu Kα characteristic radiation (wavelength = 0.154 nm). The voltage and current were set at 40 kV and 40 mA, respectively. The step size was 0.02°, and the residence time was 0.1 s. The scanning scope of 2θ was from 10 to 60°.

Fourier Transform Infrared (FTIR) Spectroscopy. The characterization of the chemical composition was performed by FTIR spectroscopy (Spectrum 100, PerkinElmer) with a resolution of 4 cm^{-1}. The samples were processed into pellets with KBr. The scanning range was 4000–400 cm^{-1}.

Morphology Studies. The morphology studies were performed with field emission scanning electron microscopy (SEM; S4800, Hitachi, Japan) with an acceleration voltage of 5 kV, and the samples were sputter-coated with Au for 40 s before SEM measurement.

Thermogravimetric Analysis. The thermal stability of the samples was investigated with a thermogravimetric analyzer (TG 209, Netzsch, Germany). A 4–5 mg sample was placed in a platinum pan and heated to 800°C under a nitrogen atmosphere at a heating rate of 10°C/min.

Density and Porosity Measurements. The porosity (*P;* %) was calculated with the following equation:[26,27]

$$P(\%) = (1 - \rho_b/\rho_s) \times 100 \quad (1)$$

where ρ_b is the bulk density, which can be obtained by the ratio of the mass to volume, and ρ_s is the skeleton density, which can be measured by pycnometry. Each sample was tested three times.

N_2 Adsorption–Desorption Measurements. The N_2 adsorption–desorption isotherms and pore size distributions of the composite aerogels were measured with a surface area and pore size analyzer (NOVA 2200e, Quantachrome). The specific

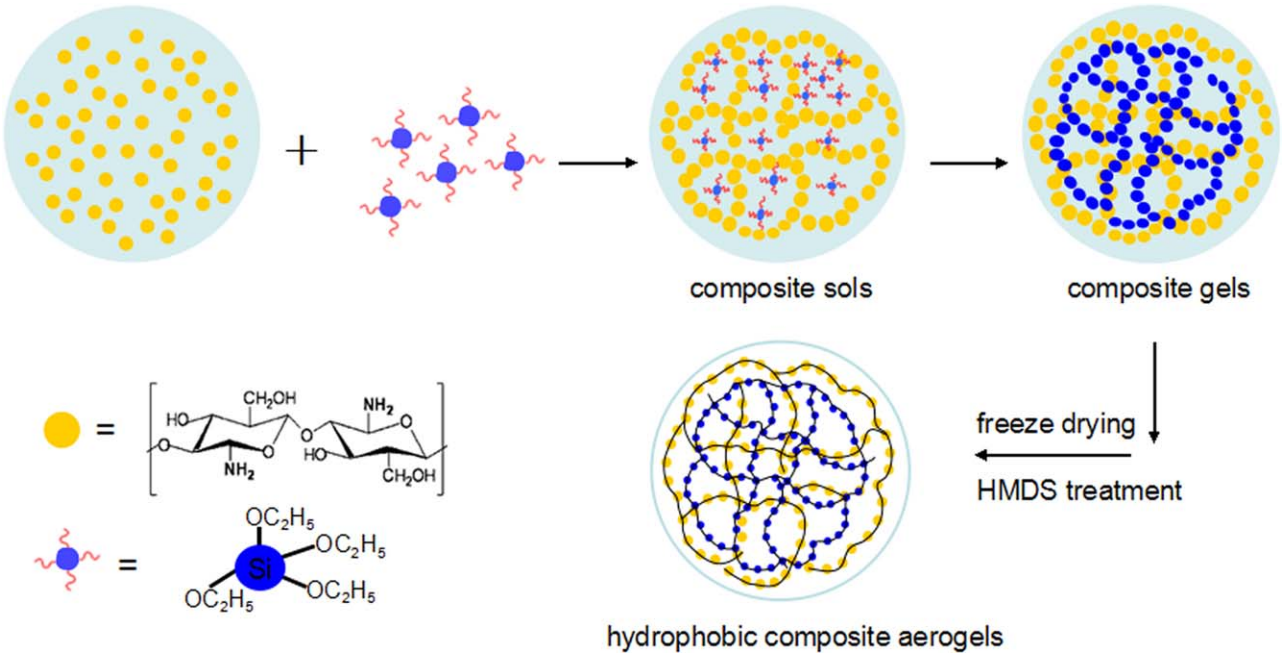

Figure 1. Schematic illustration of the formation of the composite aerogels. [Color figure can be viewed in the online issue, which is available at wileyonlinelibrary.com.]

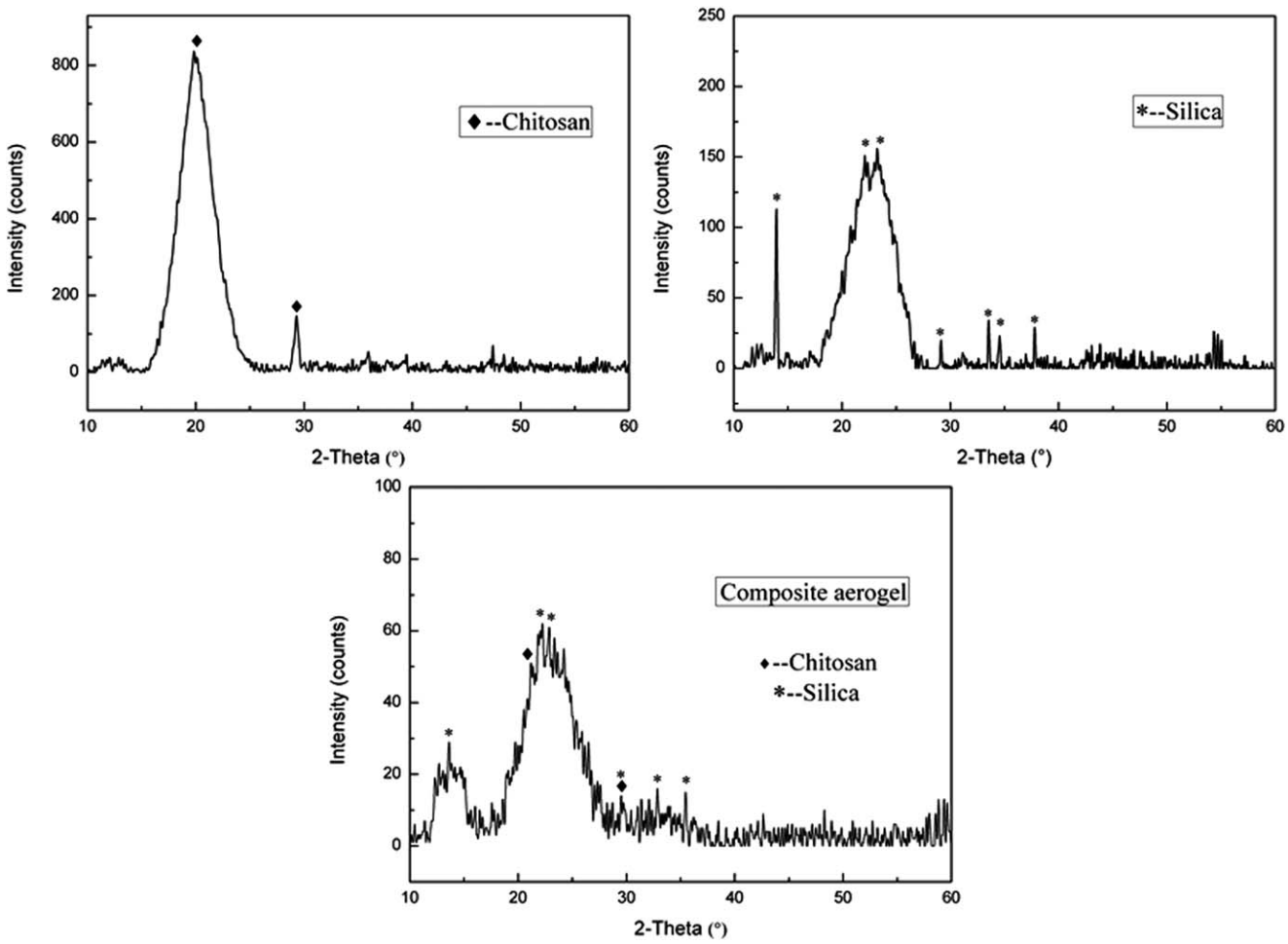

Figure 2. XRD patterns of the (a) chitosan, (b) silica aerogel (0-CS), and (c) composite aerogel (20-CS).

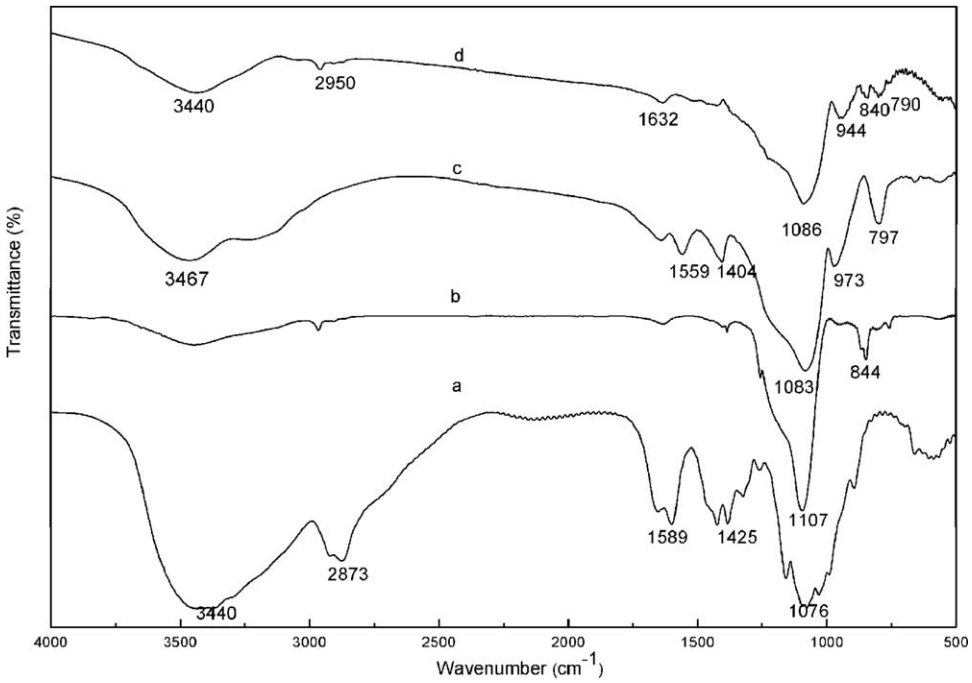

Figure 3. FTIR spectra of the (a) chitosan, (b) silica aerogel (0-CS), (c) unmodified composite aerogel, and (d) HMDS-modified composite aerogel.

surface area was obtained by the Brunauer–Emmett–Teller (BET) method. The pore diameter and pore volume were measured by the Barrett-Joyner-Halenda (BJH) nitrogen adsorption–desorption method.

Compression Resistance Tests. Because of the characteristics of the aerogels, the compression resistance could be estimated by the loading weights.[28–30] The samples were cut into small blocks and then loaded with different weights from 5 to 100 g. The compression resistance of the samples could be compared by the deformation degree.

Contact Angle Measurements. The contact angle (θ) was measured by a contact angle meter (JC2000D4, Powereach, Shanghai, China). The hydrophobicity was examined by contact angle measurements, and it was also confirmed by FTIR spectroscopy with the decreasing peak intensity corresponding to hydroxyl groups.

Oil Absorption Tests. The oil absorbency, which indicates the mass of organic liquid/oil absorbed by a unit mass of aerogel, was obtained with the following equation:

$$\Phi=(m_t-m)/m \quad (2)$$

where Φ is the oil absorbency of the aerogel, m_t is the total mass of the aerogel after absorbing oil, and m is the mass of the dried aerogel. Each sample was tested three times.

RESULTS AND DISCUSSION

The formation of the chitosan–silica composite aerogels and microstructures of the system at each stage are illustrated in Figure 1.

Chemical Composition Analysis

The XRD patterns of the chitosan, silica aerogel, and composite aerogel with 20 wt % chitosan (unless otherwise stated, the composite aerogel refers to the HMDS-modified chitosan–silica composite aerogel hereafter) are shown in Figure 2. We observed that raw chitosan had a relatively high degree of crystallinity with a sharp diffraction peak at 20° and a weak diffraction peak at 29°. The diffraction peaks of the silica aerogel were in accordance with PDF#32–0993-silica, with sharp diffraction peaks at 14, 22, and 23° and weak diffraction peaks at 25, 29, 33, and 35°. The pattern of the composite aerogel was mainly a combination of chitosan and silica, except for the fact that the intensity of both chitosan and silica diffraction peaks decreased to some extent. The coexistence of the chitosan and silica diffraction peaks indicated that the chitosan–silica composite aerogel was prepared successfully.

FTIR spectroscopy was also applied to confirm the formation and successful hydrophobic modification of the composite aerogels. Figure 3 illustrates the FTIR spectra of the chitosan, silica aerogel, unmodified composite aerogel, and HMDS-modified composite aerogel. The spectra of the original chitosan and hydrophobic silica aerogel were in accordance with previous studies.[25,27] The successful preparation of the chitosan–silica composite aerogel was verified by absorption bands appearing at 1515–1650 and 666–800 cm^{-1}, which corresponded to the bending vibrations of —NH_2 bonds from chitosan, and 830–1110 cm^{-1}, which were associated with the bending vibrations of Si—O—Si bonds and Si—O—C bonds from silica. After hydrophobic treatment, the hydroxyl group absorption band around 1404 cm^{-1} of the chitosan–silica composite aerogel was found to be very weak, and this confirmed the modification of the chitosan–silica composite aerogel.

Morphologies of Silica Aerogel, Chitosan Aerogel, and Composite Aerogel

Figure 4 shows the photographs and SEM micrographs of the silica aerogel, chitosan aerogel, and chitosan–silica composite

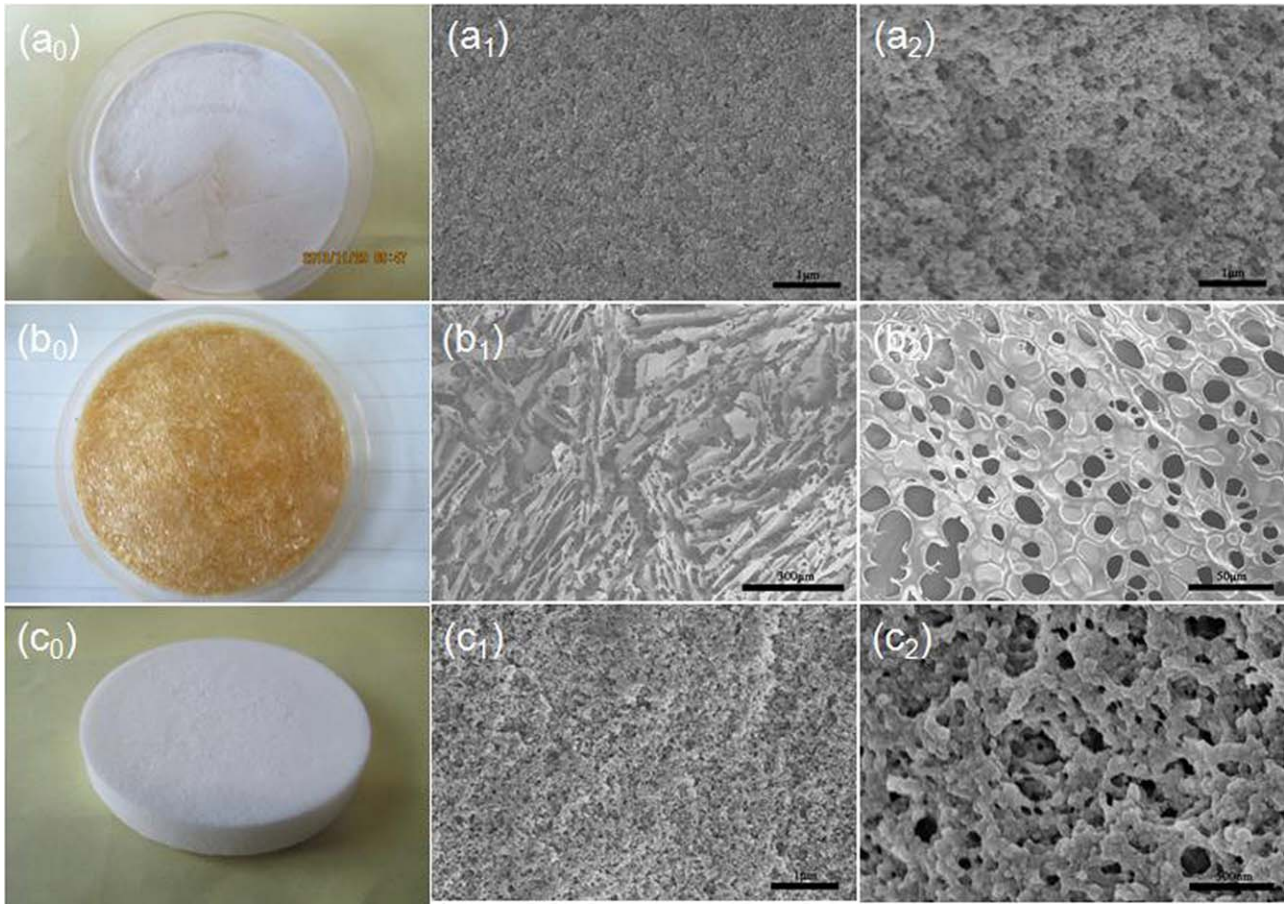

Figure 4. Photographs of the aerogels: (a_0) silica aerogel (0-CS), (b_0) chitosan aerogel (100-CS), and (c_0) chitosan–silica composite aerogel (20-CS) and SEM micrographs of these aerogels: (a_1) unmodified silica aerogel, (a_2) HMDS-modified silica aerogel, (b_1,b_2) chitosan aerogel with glutaraldehyde as the crosslinker, (c_1) unmodified composite aerogel, and (c_2) HMDS-modified composite aerogel. [Color figure can be viewed in the online issue, which is available at wileyonlinelibrary.com.]

aerogel (20-CS). We observed that compared with the unmodified silica aerogel, the silica aerogel exhibited a porous structure after the hydrophobic treatment. Chitosan aerogel with glutaraldehyde as a crosslinker had a micron-sized porous structure. In addition, chitosan–silica composite aerogel was full of large amounts of nanopores and also exhibited a looser microstructure after hydrophobic treatment.

Thermal Stability of the Composite Aerogels

The thermal stability of the silica aerogel, raw chitosan, and composite aerogels was estimated by thermogravimetric analysis. As shown in Figure 5, the weight of the silica aerogel (0-CS) decreased slightly with increasing temperature because of the loss of unreacted TEOS and the oxidization of methyl groups (—CH_3) on the surface of the modified silica aerogel.[31] The weight of chitosan decreased first (<100°C) because of the loss of moisture and then decreased largely (>260°C) which was caused by the decomposition of chitosan. With increasing chitosan content, the loss weight of the composite aerogels increased accordingly. Meanwhile, the decomposition temperature (T_d) of the composite aerogels varied with different reagent ratios. The T_d values of 20-CS and 30-CS were slightly higher than that of chitosan, whereas 10-CS had a lower T_d. The improvement of the thermal stability could be explained by a reinforcing effect on the structure of the composite aerogel when the chitosan content reached 20 wt %, and the lower T_d of 10-CS might have been because large amounts of silica particles disrupted the original intermolecular forces between the chitosan molecules.[32,33] Among all of the samples, 20-CS exhibited an optimal thermal stability with a T_d of nearly 300°C.

Porosity Characteristics of the Composite Aerogels

The bulk density and porosity of the chitosan–silica composite aerogels are summarized in Table I. The bulk density of the composite aerogels decreased constantly from 0.173 to 0.058 g/cm^3 with increasing chitosan content. Meanwhile, the porosity of the composite aerogel increased with increasing chitosan amount until a maximum porosity of 96.7% was achieved at a 20 wt % chitosan content. Interestingly, when the content of chitosan exceeded 20 wt %, further addition of chitosan did not lead to greater porosity. Instead, the porosity tended to decrease again. The constant increment and then decrease of the porosity is explained in Figure 6. From the pore size distributions, 5-CS and 10-CS had few nanopores, but the nanopores of composite aerogels tended to increase with increasing chitosan. Undoubtedly, the porosity increased with the content of chitosan. When

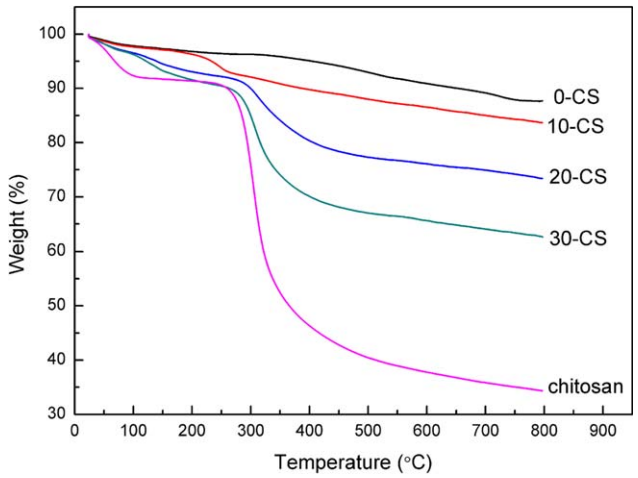

Figure 5. TGA curves of the silica aerogel (0-CS), composite aerogels (10-CS, 20-CS, and 30-CS), and chitosan. [Color figure can be viewed in the online issue, which is available at wileyonlinelibrary.com.]

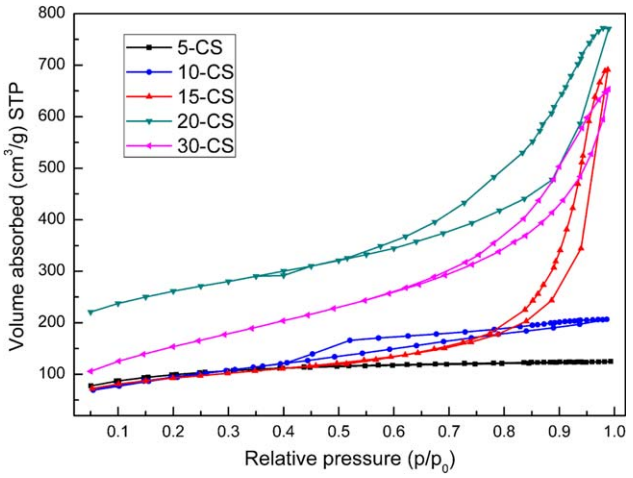

Figure 6. BJH pore size distributions of the chitosan–silica composite aerogels. p is the nitrogen pressure and p_0 is the nitrogen saturation vapor pressure [Color figure can be viewed in the online issue, which is available at wileyonlinelibrary.com.]

chitosan reached 20 wt %, a large number of nanopores (10–100 nm) was observed in the composite aerogel sample (20-CS). After that, the porosity decreased because of the decreasing nanopores. Therefore, the porosity of 20-CS was the highest among all of the samples.

Table I also exhibits the BET surface area and pore volume of the composite aerogels with different mass ratios of chitosan. The pure chitosan aerogel (100-CS) was not measured because of its micron-sized pores. It turned out that 20-CS had a relatively high surface area (618 m^2/g) and a large pore volume (1.43 cm^3/g); these increased by 315 and 101% compared with the values for 0-CS, respectively. Figure 7 shows the N_2 adsorption–desorption isotherms of the chitosan–silica composite aerogels with different reagent ratios. This indicated that the volume absorbed by 20-CS was larger than that of other samples during the nitrogen adsorption–desorption process. In conclusion, all of the previous results demonstrated that the addition of the optimal 20 wt % chitosan endowed the chitosan–silica composite aerogel with excellent adsorption performance.

Compression Resistance of the Composite Aerogels

Figure 8 shows the photographs of 0-CS, 5-CS, and 20-CS before and after the loading of weights. Before the weights were loaded, we observed that 20-CS was a little thicker; this indicated less shrinkage than in 0-CS and 5-CS. For 0-CS, a load of 2 or 10 g could easily crush the aerogel; this verified the inherent fragility of the silica aerogel. In comparison, 5-CS only had a slight compression deformation with a load of 2 g; this indicated an improvement in the mechanical strength upon the addition of 5 wt % chitosan. However, 5-CS was seriously deformed with a load of 10 g. When the amount of chitosan reached 20 wt %, the obtained composites aerogel (20-CS) exhibited hardly any deformation with a load of 2 or 10 g and only slight deformation with a load of 20 or 50 g. Here, 20-CS could even bear a load of 100 g (0.98 N) without crush. Because the weight of sample 20-CS was 14.3 mg, we concluded that 20-CS was able to support an object with almost 7000 times its own weight. Therefore, we confirmed that chitosan in the composite aerogels played an important role as a supporting skeleton and increased the mechanical properties.

Hydrophobicity and Lipophilicity

Young's equation:[34]

$$\gamma_{lv}\cos\theta=\gamma_{sv}-\gamma_{sl} \quad (3)$$

where γ_{sv}, γ_{sl}, and γ_{lv} are the interfacial tensions of the solid–vapor, solid–liquid, and liquid–vapor phases, respectively. The

Table I. Porosity Characteristics of the Composite Aerogels with Different Mass Ratios of Chitosan

Sample	Chitosan in aerogel (wt %)	Bulk density ± 0.002 g/cm³	Surface area ± 5 m²/g	Pore volume ± 0.2 cm³/g	Porosity ± 0.2%
0-CS	0	0.173	149	0.71	90.9
5-CS	5	0.145	306	0.89	92.3
10-CS	10	0.106	332	0.96	94.3
15-CS	15	0.083	452	1.01	95.6
20-CS	20	0.062	618	1.43	96.7
30-CS	30	0.071	563	1.30	96.1
100-CS	100	0.058	—	—	96.3

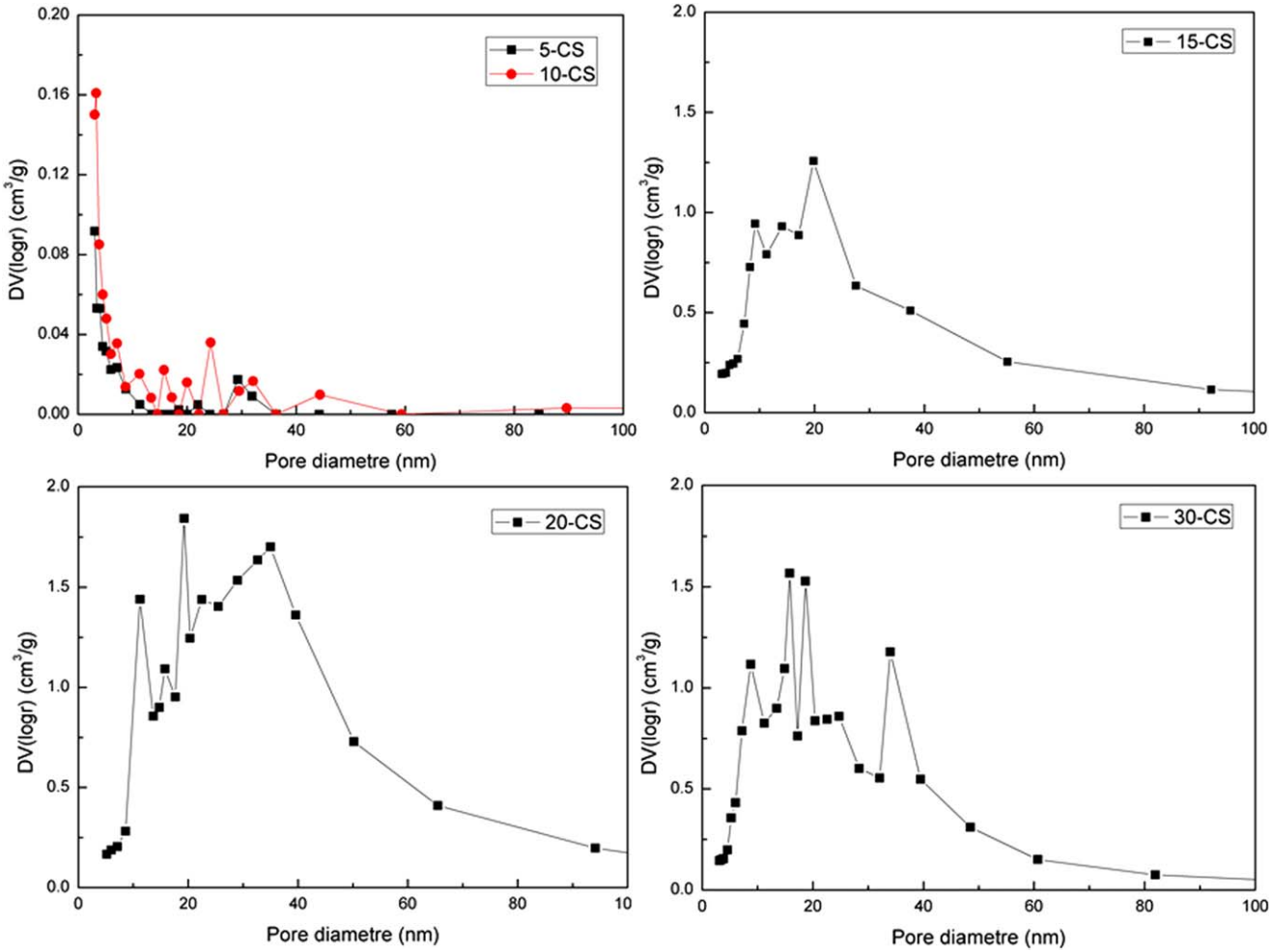

Figure 7. N_2 adsorption–desorption isotherms of the chitosan–silica composite aerogels. DV represents pore volume at certain pore diameter; DV(logr) is directly obtained from the nitrogen physisorption analysis, and it is always used as Y-axis. [Color figure can be viewed in the online issue, which is available at wileyonlinelibrary.com.]

liquid can partly wet the solid if its surface tension is larger than a critical value (γ_c), and it can wet the solid totally if its surface tension is lower than this critical value.[22] The surface free energy of the hydrophobic aerogel was lower than that of water (72.8 mN/m) but larger than that of organic solvents (ca. 18–29 mN/m); this resulted in its hydrophobicity and lipophilicity. The same sample (20-CS) was cut into two small blocks and then put in a beaker with water or an oil/water mixture, respectively. As shown in Figure 9(a), the composite aerogel floated above the water surface without any absorption, but it was wetted by arachis oil and swelled remarkably with a high absorption in the water–oil mixture. Meanwhile, the contact angle tests indicated that 20-CS had a water contact angle of 137° and an oil contact angle of 0°. These results further indicated the low density, hydrophobicity, and lipophilicity of the final composite aerogels.

Oil Absorbency Application

Chitosan–silica composite aerogels could be used as oil absorbents because of their nanoporous structure, hydrophobicity, and lipophilicity. To evaluate the oil absorption capability of the composite aerogels, the oil absorption and desorption dynamics were obtained by the measurement of the mass of aerogels after they absorbed oils at regular intervals. Several organic solvents, including pentane, hexane, acetone, dichloromethane, xylene, gasoline, and arachis oil, were applied. Figure 9(b) shows the oil absorption dynamic curves of the chitosan–silica composite aerogel with 20 wt % chitosan (20-CS). Organic liquids were absorbed at a high rate in the first 2 min, then the absorption rate turned slow, and the oil absorbency reached its maximum within 10 min.

The organic liquids were absorbed by the capillary force arising from the nanoporous structure of aerogels. The mass of liquid followed the formula:[35]

$$2\pi r\gamma \cos\theta = mg \tag{4}$$

where r is the pore radius of the aerogel, γ is the surface tension of the liquid, m is the mass of liquid absorbed by aerogel, and g is the gravity factor. In this experiment, the organic liquids wetted the aerogel totally, and therefore, the contact angle was zero. In this case, the mass of absorbed liquid was obviously

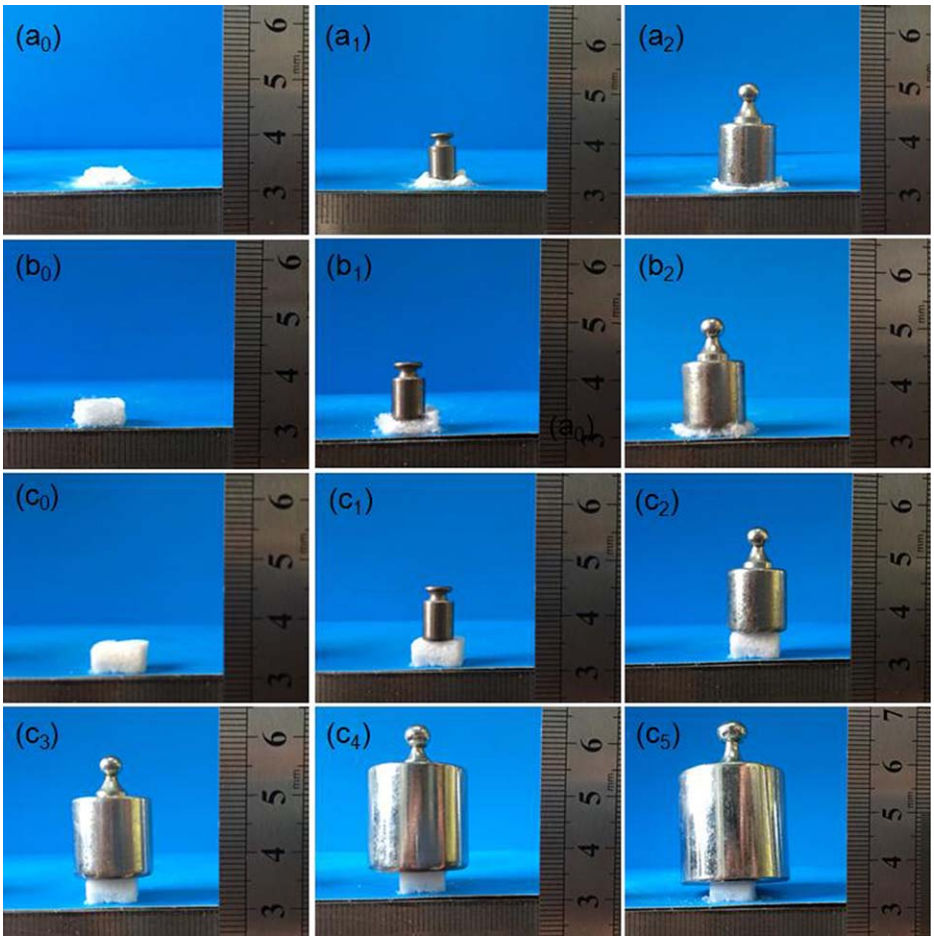

Figure 8. Photographs of the compression resistance tests: (a_0) 0-CS, (a_1) 0-CS with a load of 2 g, (a_2) 0-CS with a load of 10 g, (b_0) 5-CS, (b_1) 5-CS with a load of 2 g, (b_2) 5-CS with a load of 10 g, (c_0) 20-CS, (c_1) 20-CS with a load of 2 g, (c_2) 20-CS with a load of 10 g, (c_3) 20-CS with a load of 20 g, (c_4) 20-CS with a load of 50 g, and (c_5) 20-CS with a load of 100 g. [Color figure can be viewed in the online issue, which is available at wileyonlinelibrary.com.]

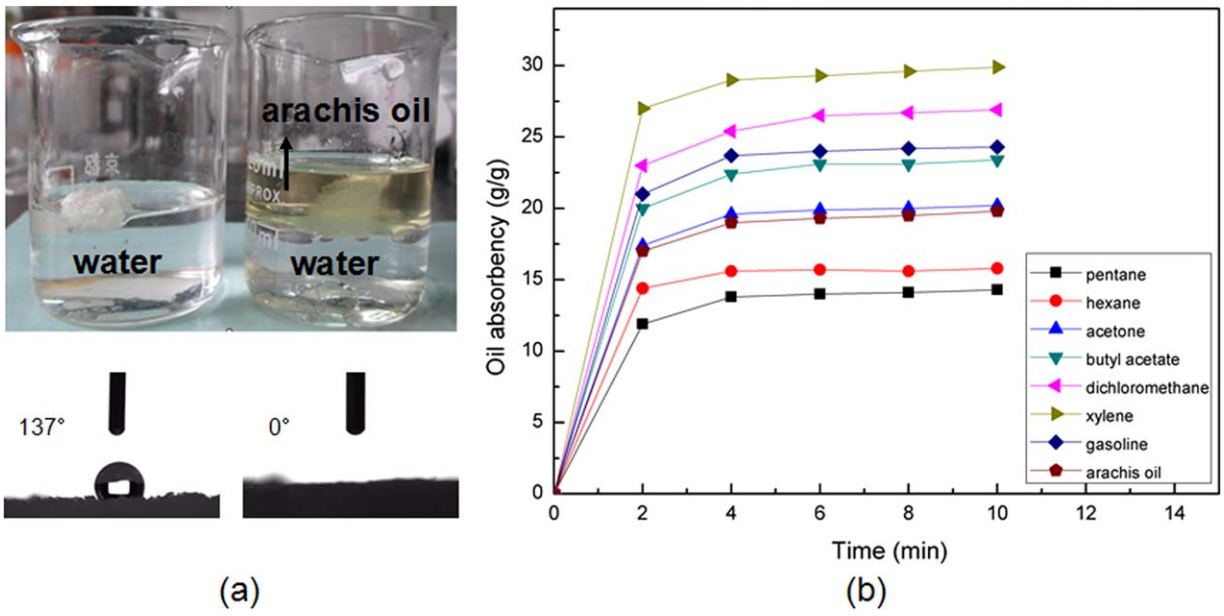

Figure 9. (a) Photographs of the composite aerogels in the water phase and oil/water mixture and (b) oil absorption dynamic curves of 20-CS. [Color figure can be viewed in the online issue, which is available at wileyonlinelibrary.com.]

Table II. Oil Absorbency of the Composite Aerogels and Surface Tension of Organic Liquids Absorbed by Aerogels at 20°C

Organic liquid/oil	Surface tension (mN/m)	Oil absorbency of the composite aerogel (g/g)				
		5-CS	10-CS	15-CS	20-CS	30-CS
n-Pentane	16.1	7.1 ± 0.1	8.2 ± 0.2	9.4 ± 0.2	14.3 ± 0.1	11.4 ± 0.2
n-Hexane	18.4	9.4 ± 0.1	9.6 ± 0.4	11.3 ± 0.2	15.8 ± 0.2	12.6 ± 0.3
Acetone	24.0	10.5 ± 0.2	11.3 ± 0.2	13.4 ± 0.1	20.2 ± 0.4	17.4 ± 0.3
Butyl acetate	25.4	12.9 ± 0.2	13.6 ± 0.1	16.1 ± 0.5	23.4 ± 0.3	18.3 ± 0.3
Dichloromethane	27.8	13.7 ± 0.2	14.6 ± 0.3	18.6 ± 0.3	26.9 ± 0.5	20.0 ± 0.5
Xylene	29.0	15.3 ± 0.1	16.0 ± 0.1	20.5 ± 0.5	30.0 ± 0.2	22.1 ± 0.2
Gasoline	—	11.5 ± 0.4	13.2 ± 0.2	17.8 ± 0.4	24.3 ± 0.6	19.5 ± 0.2
Arachis oil	—	9.7 ± 0.2	10.3 ± 0.1	14.6 ± 0.3	19.8 ± 0.1	15.7 ± 0.3

proportional to its surface tension. The surface tension of the organic solvents were different in nature; consequently, the mass of liquid absorbed by the same aerogel sample varied according to the type of liquid. As displayed in Table II, the mass of xylene and pentane absorbed by the aerogel were the largest and lowest, respectively; this accorded well with the previous formula. According to the type of organic solvents, the oil absorbency of 20-CS ranged from 14.3 to 30.0 g/g. In addition, the oil absorbency of the composite aerogels showed a tendency of first increasing to a maximum at 20 wt % and then decreasing with the addition of chitosan contents. This was totally consistent with the variation of the pore volume shown in Table I. Because of its numerous nanopores and large pore volume, 20-CS had the highest oil absorbency among all of the samples. Compared with 5-CS, the oil absorbency of 20-CS was improved by as much as 100%.

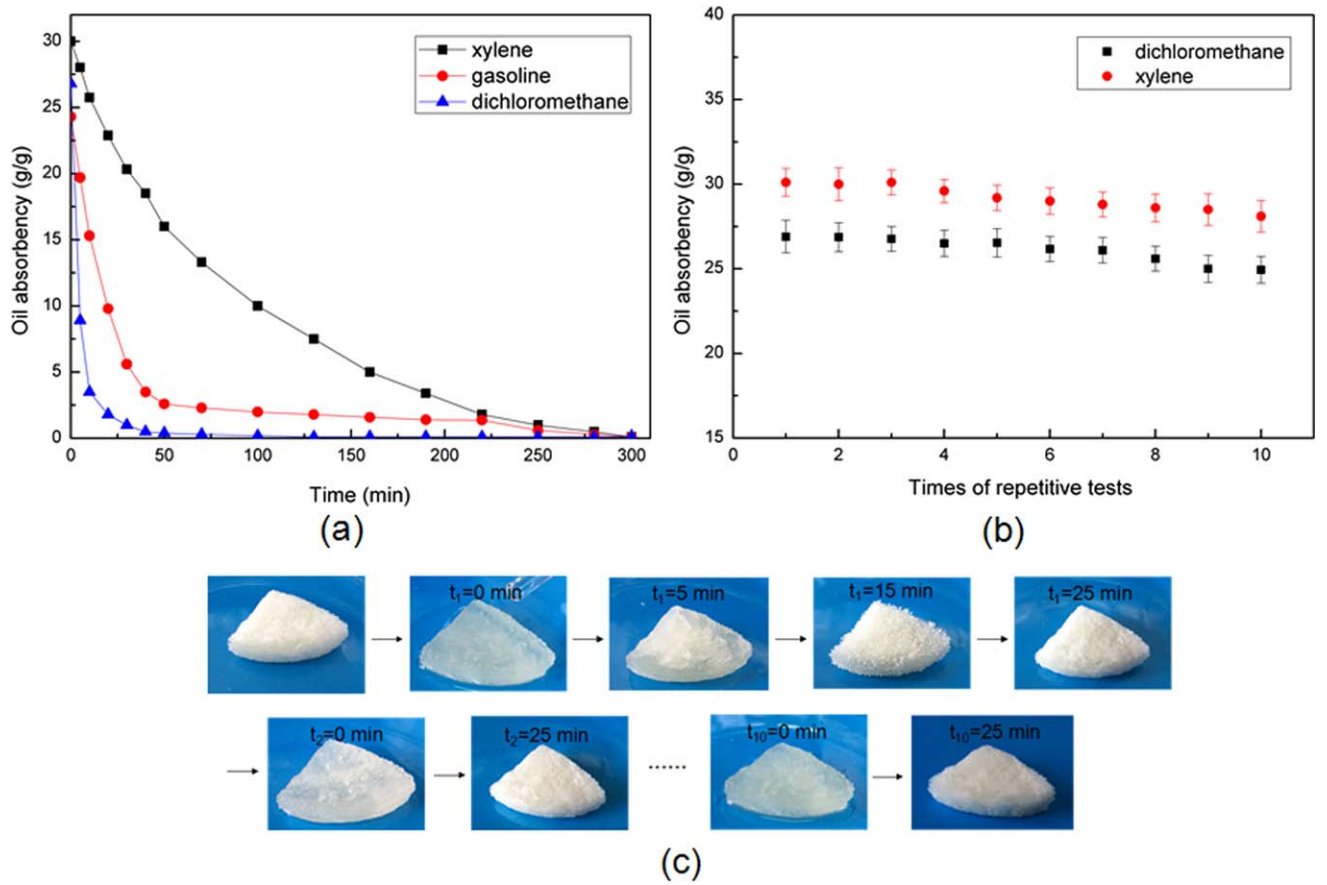

Figure 10. (a) Oil desorption dynamic curves of 20-CS, (b) oil absorbency of 20-CS for 10 cycles, and (c) photographs of the absorption and desorption process of 20-CS during the absorption of dichloromethane for 10 cycles. t_1, t_2, and t_{10} are the time of first, second and tenth cycle during the repetitive absorption tests. [Color figure can be viewed in the online issue, which is available at wileyonlinelibrary.com.]

Figure 10(a) depicts the oil desorption curves of the chitosan–silica composite aerogel (20-CS) after it absorbed three different organic liquids. Organic liquids were observed to evaporate at a high rate in the early stage; then, the rate of desorption became slow, and the oil absorbency of the aerogel decreased to nearly 0 g/g at last. The desorption of 20-CS after the absorption of dichloromethane finished within 25 min, but the desorption time with xylene as the organic liquid was almost 300 min. The differentiation of the desorption time for different organic liquids was attributed to the different characteristics of these organic liquids during the two stages in the process of desorption. In the first stage, liquid molecules moved from the interior to the surface, so it was easier for the organic liquid which had a low surface tension to arrive at the surface of the aerogel. In the second stage, the liquids evaporated from the surface by vapor pressure; this differed because of the molecular chain length, molecular weight, and so on.[36]

To take full advantage of the aerogels, the oil absorbency of 20-CS was retested 10 times. Figure 10(b) shows that the composite aerogel (20-CS) absorbed dichloromethane and xylene with a high absorbency (almost 30 and 27 g/g, respectively), and the oil absorbency remained approximately unchanged after it was reused up to 10 times; this was close to the oil absorbency of some acrylic copolymers.[37] From Figure 10(c), the absorption–desorption process of 20-CS was observed with dichloromethane as the organic solvent. 20-CS could be reused without any deformation 10 times; this further demonstrated that it had great potential to be an efficient and recyclable oil absorbent.

CONCLUSIONS

In this study, hydrophobic and nanoporous chitosan–silica composite aerogels with low density, high porosity, and superior oil absorbency were prepared feasibly and simply by a typical sol–gel process and a two-step hydrophobic treatment. The composite aerogels exhibited a nanoporous structure, together with a large specific surface area and high pore volume; this could be concluded from the SEM micrographs and nitrogen physisorption analysis. In addition, the composite aerogels were thermally stable up to nearly 300°C and also had relatively high compression resistance; this confirmed that chitosan in the composite aerogels played an important role as a skeleton support. Importantly, the hydrophobic treatment made the composite aerogels hydrophobic, with a water contact angle of 137° but lipophilic with an oil contact angle of 0°. After that, the oil absorption and desorption tests showed that composite aerogels could reach equilibration of oil absorption within 10 min and had relatively high oil absorbency as much as 30 g/g. Therefore, the chitosan–silica composite aerogels in this study have a bright future in the application of oil absorption.

ACKNOWLEDGMENTS

This work was financially supported by the Natural Science Foundation of China (contract grant number 21172167).

REFERENCES

1. Hrubesh, L. W. *Chem. Ind.-London* **1990**, *24*, 824.
2. Yavari, F.; Koratkar, N. *J. Phys. Chem. Lett.* **2013**, *3*, 1746.
3. Wu, Z. S.; Yang, S.; Sun, Y.; Parvez, K.; Feng, X. L.; Muüllen, K. *J. Am. Chem. Soc.* **2012**, *134*, 9082.
4. Ricci, A.; Bernardi, L.; Gioia, C.; Vierucci, S.; Robitzer, M.; Quignard, F. *Chem. Commun.* **2010**, *46*, 6288.
5. Dou, B.; Li, J.; Wang, Y.; Wang, H.; Ma, C.; Hao, Z. *J. Hazard. Mater.* **2011**, *196*, 194.
6. Wang, H.; Yuan, X. *Environ. Sci. Pollut. R.* **2014**, *21*, 1248.
7. Aliev, A. E.; Oh, J. Y.; Kozlov, M. E.; Kuznetsov, A. A.; Fang, S. L.; Fonseca, A. F.; Ovalle, R.; Lima, M. D.; Haque, M. H.; Gartsterin, Y. N.; Zhang, M.; Zakhidov, A. A.; Baughman, R. H. *Science* **2009**, *323*, 1575.
8. Dong, X. C.; Xu, H.; Wang, X. W.; Huang, Y. X.; Chan-Park, M. B.; Zhang, H.; Wang, L. H.; Huang, W.; Chen, P. *ACS Nano* **2012**, *6*, 3206.
9. Lee, J. K.; Gould, G. L. *J. Sol–Gel Sci. Technol.* **2007**, *44*, 29.
10. Wu, Z.; Li, C.; Liang, H.; Chen, J.; Yu, S. *Angew. Chem. Int. Ed.* **2013**, *125*, 2997.
11. Hoepfner, S.; Ratke, L.; Milow, B. *Cellulose* **2008**, *15*, 121.
12. Scanlon, S.; Aggeli, A.; Boden, N.; Koopmans, R. J.; Brydson, R.; Rayne, C. M. *Micro Nano Lett.* **2007**, *2*, 24.
13. Ingale, S. V.; Sastry, P. U.; Wagh, P. B.; Tripathi, A. K.; Rao, R.; Tewari, R.; Rao, P. T.; Patel, R. P.; Tyagi, A. K.; Gupta, S. C. *Mater. Chem. Phys.* **2012**, *135*, 497.
14. Baumann, T. F.; Gash, A. E.; Chinn, S. C.; Sawvel, A. M.; Maxwell, R. S.; Satcher, J. H., Jr. *Chem. Mater.* **2005**, *17*, 395.
15. Cong, H.; Ren, X.; Wang, P.; Yu, S. *ACS Nano* **2012**, *6*, 2693.
16. Liang, H.; Guan, Q.; Chen, L.; Zhu, Z.; Zhang, W.; Yu, S. *Angew. Chem. Int. Ed.* **2012**, *51*, 5101.
17. Pojanavaraphan, T.; Liu, L.; Ceylan, D.; Okay, O.; Magaraphan, R.; Schiraldi, D. A. *Macromolecules* **2011**, *44*, 923.
18. Wang, Y. X.; Al-Biloushi, M.; Schiraldi, D. A. *J. Appl. Polym. Sci.* **2012**, *124*, 2945.
19. Schaefer, D. W.; Keefer, K. D. *Phys. Rev. Lett.* **1986**, *56*, 2199.
20. Hæreid, S.; Dahle, M.; Lima, S.; Einarsrud, M. A. *J. Non-Cryst. Solids* **1995**, *186*, 96.
21. On, N. K.; Rashid, A. A.; Nazlan, M.; Hamdan, H. *J. Appl. Polym. Sci.* **2012**, *124*, 3108.
22. Gurav, J. L.; Rao, A. V.; Nadargi, D. Y.; Park, H. *J. Mater. Sci.* **2010**, *45*, 503.
23. Parale, V. G.; Mahadik, D. B.; Kavale, M. S.; Rao, A. V.; Wagh, P. B.; Gupta, S. C. *Soft Nanosci. Lett.* **2011**, *1*, 97.
24. Robitzer, M.; Renzo, F. D.; Quignard, F. *Micropor. Mesopor. Mater.* **2011**, *140*, 9.
25. Kumar, S.; Dutta, J.; Dutta, P. K. *Int. J. Biol. Macromol.* **2009**, *45*, 330.
26. Sarawade, P. B.; Kim, J.; Hilonga, A.; Kim, H. T. *Solid State Sci.* **2010**, *12*, 911.
27. Bhagat, S. D.; Rao, A. V. *Appl. Surf. Sci.* **2006**, *252*, 4289.
28. Bryning, M. B.; Milkie, D. E.; Islam, M. F.; Hough, L. A.; Kikkawa, J. M.; Yodh, A. G. *Adv. Mater.* **2007**, *19*, 661.

29. Kohlmeyer, R. R.; Lor, M.; Deng, J.; Liu, H.; Chen, J. *Carbon* **2011**, *49*, 2352.

30. Xu, Y.; Sheng, K.; Li, C.; Shi, G. *ACS Nano* **2010**, *4*, 4324.

31. Parvathy Rao, A.; Rao, A. V. *J. Non-Cryst. Solids* **2009**, *355*, 2260.

32. Pavan, F. A.; Franken, L.; Moreira, C. A.; Costa, T.; Benvenutti, E. V.; Gushikem, Y. *J. Colloid Interface Sci.* **2001**, *241*, 413.

33. Laachachi, A.; Leroy, E.; Cochez, M.; Ferriol, M.; Cuesta, J. *Polym. Degrad. Stab.* **2005**, *89*, 344.

34. Adamson, A. W. Physical Chemistry of Surfaces; Wiley-Interscience: New York, **1976**.

35. Newman, F. H.; Searle, V. H. L. The General Properties of Matter; Orient Longmans: London, **1957**.

36. Rao, A. V.; Hegde, N. D.; Hirashima, H. *J. Colloid Interface Sci.* **2007**, *305*, 124.

37. Fang, P.; Mao, P. P.; Chen, J.; Du, Y.; Hou, X. *J. Appl. Polym. Sci.* [Online early access] **2014**, *131*. DOI: 10.1002/APP.40180. Published Online: http://onlinelibrary.wiley.com/doi/10.1002/app.40180/abstract.